Journal of Casting & Materials Engineering Vol. 6 No. 2 (2022) 33–38
https://doi.org/10.7494/jcme.2022.6.2.33

A Novel Approach to Quantifying the Effect of the Density of Sand Cores on Their Gas Permeability

Dinesh Sundaram*, József Tamás Svidró, Judit Svidró, Attila Diószegi

Jönköping University School of Engineering, Department of Materials and Manufacturing, Gjuterigatan 5, Box 1026, SE-55111 Jönköping, Sweden
**email: dinesh.sundaram@ju.se*

Received: 29 October 2021/Accepted: 22 February 2022/ Published online: 30 March 2022.
This article is published with open access at AGH University of Science and Technology Press.

Abstract

The density of moulding mixtures used in the foundry industry plays a significant role since it influences the strength, porosity, and permeability of moulds and cores. The latter is routinely tested in foundries using different solutions to control the properties of the moulding materials that are used to make moulds and cores. In this paper, the gas permeability of sand samples was measured using a custom-made setup to obtain the gas permeability in standard units instead of the usual permeability numbers (PN) with calibrated units. The aim of the work was to explore the effect of density variations in moulding materials on their gas permeabilities. Permeability in this work is quantified in SI units, square metres [m^2]. The setup works based on Darcy's law and the numbers obtained from the measurements can be used to deduce the gas permeability, *k*, of a sample. Two furan resin bonded mixtures with the same grain size distribution were hand-rammed with varying compaction forces to obtain a variation in density. Cylindrical samples (50 × 50 mm) were prepared using a silica sand aggregate sourced from a Swedish lake. The results of the measurement provided the difference in gas permeability between the samples that have varying densities. The results of permeability were then extrapolated by modifying the viscosity value of the air passed through the sample. In order to find the effect of apparent density variation on the pore characteristics of the samples, mercury intrusion porosimetry (MIP) was also performed. The results were in line with the gas permeability measurements.

Keywords:

compaction, density, furan sand, gas permeability, porous media

1. INTRODUCTION

Sand casting, one of the oldest and most versatile manufacturing processes, involves pouring molten metal into a mould cavity that is designed and shaped according to the structure and dimensions of the finished form of the component [1]. Casting methods using aggregates can be divided into two main types: non-permanent molds made by permanent patterns or non-permanent patterns. Of these two, high volume production is achieved using non-permanent/expendable moulds with permanent patterns [1]. Cores are parts of these moulds that serve the purpose of creating hollow cavities or shapes inside the cavity where patterns cannot be used [2]. Cores are prepared by binding aggregate material either using organic or inorganic binder. They are usually accompanied by the addition of a catalyst material depending on the type of the resin and process. Since they involve multiple components, they are termed binder systems [3].

Hand-ramming is an important process in the foundry industry for small volume production and prototyping. It involves the manual compaction of sand grains already mixed with the binding agents. The role of compaction or ramming is significant for several reasons. Among other things, compaction determines the density, and permeability of the moulding material. Smaller cores are compacted by compressed air and, for larger moulds and cores, pneumatic rammers are commonly used. On the industrial scale, machine compaction methods such as compression, injection and core shooting are used. Moulds are commonly manufactured using methods like bench moulding (for low production rates), machine moulding (high volume production), pit moulding (large castings) and floor moulding (medium sized castings) [4]. During the casting process, the moulds and cores must withstand heat shock and pressure in the system. If the gases formed during the thermal decomposition find a way to the liquid metal, gas related defects such as blow holes will appear in the casting. Hence gas-permeability of cores and moulds affects the casting quality and is a critical parameter [5]. In this work, the density of furan no-bake sand cores was varied by altering the compaction force during hand ramming. Gas permeability was measured using a custom-made measurement setup that provides numbers in standard units of square metres [m^2].

2. BACKGROUND

The density of sand used for foundry purposes are measured in different forms. Loose, dry and free flowing sand bulk density is measured using a 100 ml graduated cylinder and the procedure for testing this parameter is provided by the AFS Mold and Core Test Handbook [6]. On the other hand, the apparent density of solid moulds is measured using the direct relationship between the mass and the volume of the moulds and cores. Gas permeability of moulds are dependent on several factors. On a micro-scale, properties of the sand grains like the grain size and shape influence the permeability. On a macroscopic level, properties of the mould/core such as the apparent density and the resulting porosity of the sample influence the permeability. In this study, the compaction force was varied while preparing samples to achieve a difference in the apparent density, and the resulting differences in gas permeability this variation caused was quantified.

Gas permeability has not been modelled extensively for foundry cores and moulds. Several researchers from other fields have worked on predicting the gas permeability of sandstones, soil and other rocks using parameters such as grain size distribution, porosity etc. [7, 8]. Permeability prediction from porosimetry data has also been widely carried out in other fields, such as earth sciences and geothermal engineering. Ettemeyer et al. [7] measured the gas permeability of foundry cores that are 3D-printed. In their work, the measured gas permeability data were used to predict the behaviour of the sand cores, when high temperature gases passed through them.

Dańko et al. [9] studied the core properties prepared from core shooters using a custom method. Of the properties that were studied, the effect of shooting pressure, rate of filling, and the apparent density were the primary focus for different sand grain types. In another related work, Dańko worked on establishing the effect of grain size distribution on the bending strength and apparent density of commercially shot foundry samples [10]. It is also known from research in the field of petrochemical and geothermal sciences that permeability is more dependent on the pore characteristics than the porosity itself. In consolidated media there could be instances where samples that may be more porous but could have lesser interconnected pores and therefore having lower gas permeability [11]. The authors of the current work performed mercury intrusion porosimetry (MIP) measurements to reveal the pore characteristics of furan no-bake cores in an earlier study. In that work the authors quantified the effect of grain size distribution on the gas permeability of foundry cores and identified a certain threshold limit for the permeability after which the reduction in permeability were not significant [12]. The authors also identified the importance of pore characteristics of furan no-bake cores and its effect on the gas permeability. In the current work presented, the effect of apparent density on the gas permeability were studied. It is important to quantify the pore characteristics of a porous material, because they play a significant role on the gas transport properties of the sample and hence it is analysed using MIP in this study.

3. MATERIALS AND METHODS

For this study, foundry grade silica sand sourced from a Swedish lake was used as the aggregate material. The sand is widely used by the foundry industry in Sweden. The grain size distribution is shown in Figure 1. The grain size distribution and the average grain size were determined according to Swedish standards.

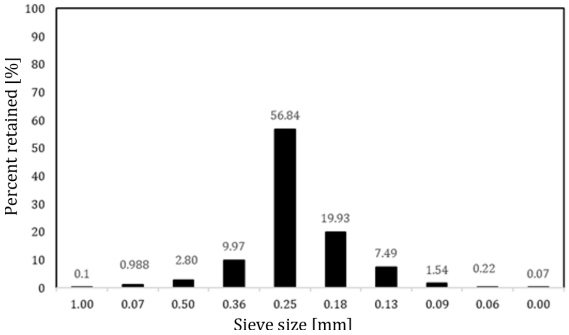

Fig. 1. Grain size distribution of the silica sand used

2% (of the mass of sand) of furan resin was added to the sand along with 40% (of the mass of the resin) sulphonic acid-based catalyst and mixed. The mixture was then hand-rammed with a custom-made rammer and tube setup. A known mass of sand was inputted into the tubes and the compaction force was varied such that the density of the samples also varied. The compaction force was not measured. The samples prepared were of the standard cylindrical geometry (50 × 50 mm) that is used widely for foundry sand testing. The curing time was 24 hours for both samples. The properties of the samples are shown in Table 1.

Table 1
Properties of the samples prepared and measured for permeability

Sample	Mass [g]	Volume [cm^3]	Density [g/cm^3]	Average grain size [mm]
A	135.12	99.73	1.39	0.31
B	149.62	99.83	1.51	

The samples were evaluated in three steps. First, gas permeability measurements were conducted using a custom-made setup that utilizes Darcy's law. The cylindrical core is enclosed in an air-tight setup that allows air (at room temperature) to flow through the specimen from one end to the other end. The pressure difference building up was measured using a differential pressure sensor. The velocity of the air was also measured on the outlet side using a mass flow sensor. The working principle and more detailed governing calculations can be found in a previous work published [13].

In the second step, the obtained gas permeability numbers were used to reveal the hypothetic effect of temperature on the gas permeability of the samples. This provides information about how the sand mixture might behave when the

temperature of the passing gas is higher (which is close to the reality when it comes to casting processes). However, the calculation assumes that the decomposition of the furan resin does not have an effect on the pore characteristics, since the resin and catalyst content is low both in mass and volume fraction when compared to the sand grains. This assumption has been previously made by researchers while measuring gas permeability [14, 15].

In the third step, the samples were then analysed using mercury intrusion MIP, using a Micro metrics Autopore III 9410.

This method provided data on the porosity, pore size distribution, pore area and other important pore characteristics. The 50 × 50 mm, cylindrical samples were cut, and three specimens from the central area of each cylinder were then machined out, according to Figure 2.

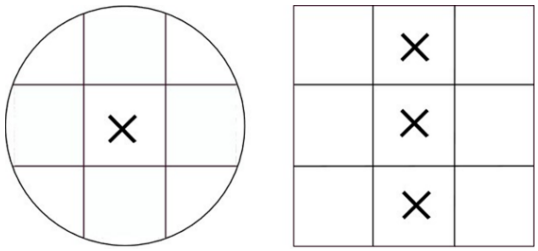

Fig. 2. Cylindrical samples were cut and the pieces for the MIP marked with a cross mark

4. RESULTS AND DISCUSSION

4.1. Permeability results

The ratio of volumetric flow rate of the air, Q in cubic metres on seconds that is measured at the outlet to the cross-sectional area, A in in squar metres of the sample is plotted (x-axis) as a function of the ratio of the differential pressure, dP in Pascals to the length of the sample, L in meters in the y-axis. Q/A plotted against dP/L for the two samples are superimposed and shown in Figure 3. From the slope of these plots, gas permeability is calculated with the help of the dynamic viscosity of air. The dynamic viscosity of the air that is passed through the sample is 1.85E-5 kg/ms [16]. A total of four measurements were performed for each sample studied and the mean with the standard deviation was calculated. The standard deviation numbers for these measurements could be found in Table 2.

The slope of the sample A is visibly steeper and has a higher gas permeability. This is expected as Sample A has a density of 1.39 g/cm^3 and it is the lower of the two samples studied. The slope of sample B is smaller than the slope of A. Sample B had a density of 1.51 g/cm^3. The air flow rate per unit area is lesser for sample B and shows that the sample is less permeable. The gas permeability values of the measured samples are presented in Figure 4. The mean gas permeability and the standard deviation results are presented in Table 2.

It can be seen that the standard deviation for sample B was much higher than Sample A. The results show that the gas permeability for Sample A was higher with $5.26 \cdot 10^{-12}$ m^2 as the mean value of four measurements. Gas-permeability of Sample B which had a higher density, eventuated in lower gas-permeability of $1.43 \cdot 10^{-12}$ m^2. The background of these findings were evaluated further by means of MIP tests.

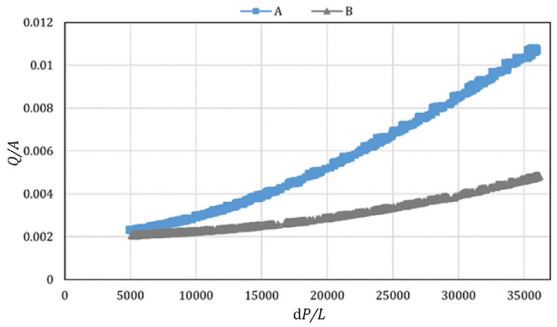

Fig. 3. Volumetric flow rate divided by the area of cross-section of the sample(y-axis)plotted against the differential pressure divided by the length of the sample

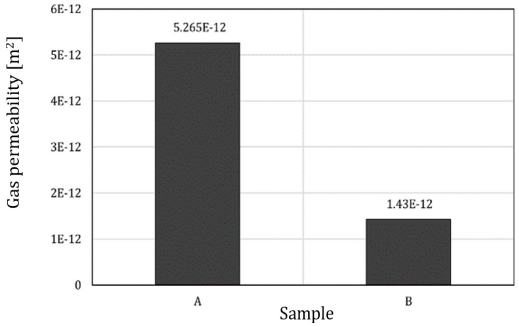

Fig. 4. Gas permeability of the measured samples A and B

Table 2
The mean gas permeability and the standard deviation results

Parameter	Sample A	Sample B
Apparent density [g/cm^3]	1.39	1.51
Gas permeability [m^2]	5.265E-12 ±0.09	1.43E-12 ±0.18
Measurement 1	5.14E-12	1.61992E-12
Measurement 2	5.24E-12	1.19667E-12
Measurement 3	5.29E-12	1.61045E-12
Measurement 4	5.39092E-12	1.34216E-12

4.2. Permeability calculated for higher temperatures based on Darcy's law

Darcy's law provides a proportionality between the volumetric flow rate of a porous material and the pressure gradient of the material when a fluid passes through [17]. The law also includes the dimensions of the sample measured such as

the area of the sample and length. Since fluid viscosity plays a significant role in the flow characteristics, the law also includes dynamic viscosity. Darcy's law can be written as in following equation, where k/μ can be obtained from the plots presented in Figure 3.

$$\frac{Q}{A} = \frac{k}{\mu} \cdot \frac{dP}{L}$$

where:

Q – volumetric flow rate of air;
A – cross-sectional area of the sample;
k – permeability;
μ – dynamic viscosity;
dP – differential pressure across the sample;
L – length of the sample.

The dynamic viscosity μ at room temperature [16] was used to determine the gas permeability of the material. To study the effect of fluid temperature on the gas permeability, the dynamic viscosity for higher temperatures [16] was considered and are incorporated in Darcy's law. The dataset for the extrapolation was based on Table 3. Using the flow characteristics measured from the experiments the gas permeability is calculated for higher temperatures. The need for such an estimation comes from the fact that the actual gases evolving during the casting process are higher than room temperature. The dynamic viscosity of a fluid affects the way it flows through the pores and the pressure difference it creates when it flows from one end to the other. Hence during the gas evolution process, when the high temperature volatile compounds try to escape the mould/core, the effect of dynamic viscosity must be taken into account. Figure 5 shows the effect of air temperature on the gas permeability which is calculated from the increasing dynamic viscosities of air. The measured permeability values (from the first measurement) of both samples A and B were used for the calculation.

From the results it can be seen that high temperature permeability sensitivity is predominant for Sample A, which had a lower room temperature permeability.

The results show how significantly the temperature of the air passing through the sand grains can affect the gas permeability. During the casting process, the temperature of the gaseous volatile substances releasing can be quite high. From the above results, one can notice that the higher the temperature, the higher the gas permeability. Apart from the effect of the dynamic viscosity, the degradation of the core itself due to the decomposition of the binder system could also change the pore structure of the moulding material, both these factors might have a significant effect the overall permeability of the core. However, in-situ experiments where simultaneous measurement of binder system decomposition and changes in pore structure are not available today, however such understandings are needed to evaluate the significance of the phenomena discussed above. The dynamic viscosity of air increases linearly and hence the gas permeability is also seen to have increased linearly.

Table 3
Effect of air temperature on the permeability of samples

Air temperature [°C]	Dynamic viscosity, [kg/ms]	Permeability k [m^2]	
		Sample A	Sample B
20	1.82E-05	5.14E-12	1.62E-12
100	3.24E-05	9.12E-12	2.88E-12
200	4.95E-05	1.39E-11	4.39E-12
300	6.87E-05	1.93E-11	6.10E-12
400	8.95E-05	2.52E-11	7.94E-12
500	1.11E-04	3.12E-11	9.85E-12
600	1.35E-04	3.80E-11	1.20E-11
700	1.59E-04	4.47E-11	1.41E-11
800	1.85E-04	5.21E-11	1.64E-11
900	2.12E-04	5.97E-11	1.88E-11
1000	2.39E-04	6.73E-11	2.12E-11

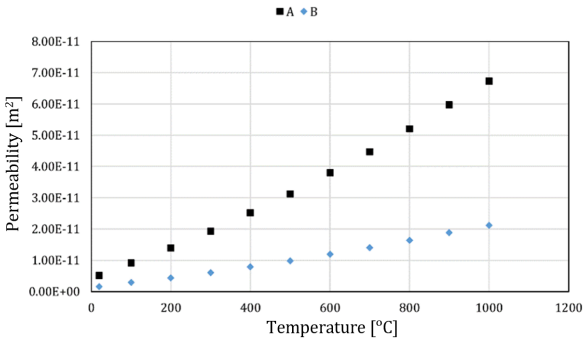

Fig. 5. The effect of air temperature on the gas permeability of the furan sand sample

4.3. MIP results

The results presented below are from the average of two samples from A (A1 and A2) and three samples from B (B1, B2 and B3). The sample A3 is not included in the results because of an unexpected error during the mercury intrusion process. The differential intrusion pore volume plotted against the mean pore diameter (with a logarithmic scale for the mean pore diameter) is shown in Figure 6.

From Figure 6a, it can be seen that both the samples show a bimodal pore size distribution. Both have pores in the size range of 300–0.01 μm. However, Sample B had a significantly higher amount of smaller pores. These smaller pores fall under the mesopores category according to IUPAC [18] classification.

a)

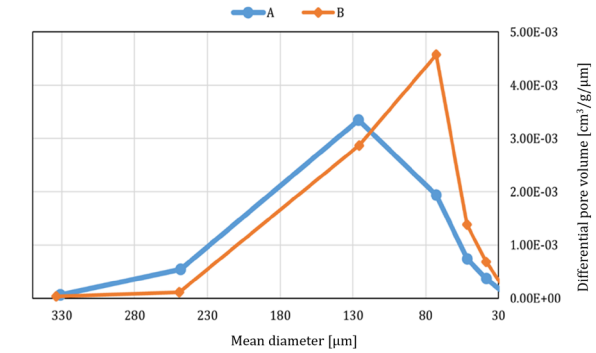

b)

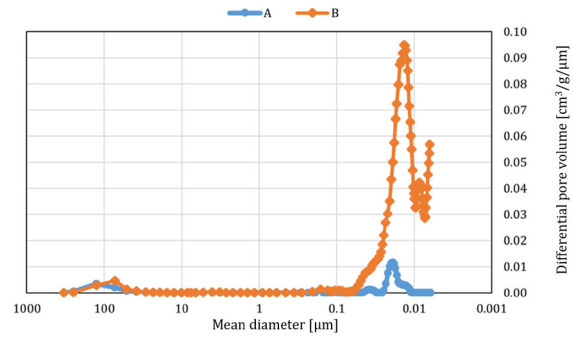

Fig. 6. The differential pore volume curve plotted as a function of the mean pore diameter (a). The first peak of Figure 6a is presented in a linear scale showing the difference in pore (b)

To discuss the pore size distribution more elaborately (Fig. 6b), which had the differential pore volume plotted against the mean pore diameter with a linear axis is presented. The area under the curve represents the pore volume of the sample measured for a particular wide pore radius. Sample B had a lower concentration of larger pores of 230–130 µm. Sample A, on the other hand, had a higher number of larger pores and a lower concentration of smaller pores both in the range of 130–80 µm and 0.1–0.009 µm. The curves showed that, a variation can be observed between sample A and B in terms of the inflection point (which could be considered the critical pore diameter). Sample A had a critical pore diameter of 130 µm, while B had a critical pore diameter of 72 µm. Parameters such critical pore diameter, concentration of the pores and the distribution clearly indicate the difference in pore characteristics and its effect on the permeability of the samples. Sample A which had an overall higher porosity, higher large pore concentration and a higher critical pore diameter exhibited higher permeability. While sample B which had a lower porosity, relatively fewer macropores and a lower critical pore diameter exhibited lesser permeability. It is, however, interesting to see the significantly higher amount of meso-micro pores in Sample B. The effect of these smaller pores on the permeability is also a factor to analyse. Sample B, which had a higher apparent density and greater degree of compaction, exhibits more micropores than Sample A. Cumulative pore volume plots or incremental pore volume plots for the two samples are shown in Figure 7.

It is evident from the cumulative pore volume curve that Sample A had a higher overall porosity and hence higher permeability. Table 4 presents the porosimetry results and the permeability of the specimens. From the results of MIP, it is clear that compaction affects the pore characteristics and the structure of the pores in foundry moulds and cores.

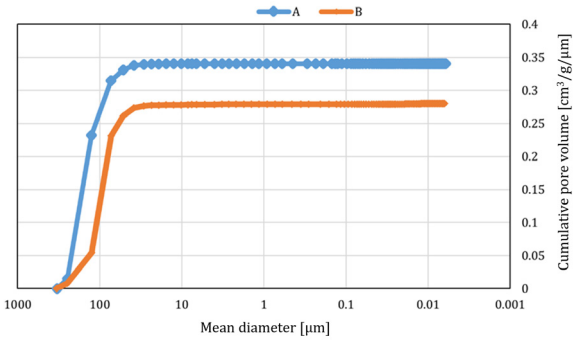

Fig. 7. Cumulative pore volume plots for sample A and B

Table 4
The pore characteristics of the samples measured using mercury intrusion porosimetry

Property	Sample A	Sample B
Apparent density [g/cm³]	1.39	1.51
Pore volume [cm³/g]	0.34	0.27
Median pore diameter [µm]	101	69
Porosity [vol. %]	47.5	43.3
Gas permeability [m²]	$5.26 \cdot 10^{-12}$	$1.43 \cdot 10^{-12}$

5. CONCLUSIONS

The presented work aimed at quantifying gas permeability when the compaction rate varied and samples with varying apparent densities are obtained. The quantification of permeability was done using a custom-made setup that provides results in standard permeability units, square metres [m²]. The results show that the permeability decreased from $5.26 \cdot 10^{-12}$ m² to $1.43 \cdot 10^{-12}$ m² for samples that increased in density from 1.39 g/cm³ to 1.51 g/cm³. The effect of sample density on the permeability was quantified and the reduction in gas permeability was measured in standard units, square metres [m²]. The effect of the temperature of the air on gas permeability was also calculated using the experimental results, with the obtained room temperature gas permeability of one measurement from both Sample A and B. From these results it is clear that gas permeability can significantly increase when air temperature is higher. Hence, when considering the gas permeability values for modelling gas evolution processes in castings, higher gas permeability numbers must be considered so that any underestimation of the amount and rate of gases that the cores could evacuate is avoided.

Results from mercury intrusion porosimetry complimented the results of gas permeability. They showed that the pore characteristics change significantly when the apparent density and compaction is higher for furan no bake sand cores. The number of smaller pores increased significantly with compaction while the critical pore diameter decreased with the increase in apparent density. It not only decreases porosity, but also decreases the average pore size. Porosity affects the permeability at a macro-level, but pore characteristics such as the amount of micro-pores, the diameter of the pores and the interconnectivity of the pores also play an important role in gas permeability. However, it will be interesting to see the effect of increased micro-pores on the gas permeability of foundry samples in the future.

Acknowledgements

The present work is part of the synergy project Lean and sustainable design and production of cast iron components. The work was financed by the Swedish Knowledge Foundation. Cooperating parties in the project are Jönköping University, Scania CV AB, Volvo Group Trucks Technology AB, SKF Mekan AB and SinterCast AB.

REFERENCES

[1] Stoll H. (2009). *Casting design and performance*. Materials Park, OH: ASM International.
[2] Bermudo C., Martín-Béjar S., Trujillo F.J. & Sevilla L. (Eds.). (2019). Use of Additive Manufacturing on Models for Sand Casting Process. *Advances on Mechanics, Design Engineering and Manufacturing II*, 359–369. Doi: https://doi.org/10.1007/978-3-030-12346-8_35.
[3] Campbell J., Svidró J.T. & Svidró J. (2017). Molding and Casting Processes (190–206). In: https://doi.org/10.31399/asm.hb.v01a.a0006297.
[4] Singh R. (2006). *Introduction to basic manufacturing process and workshop technology*. New Delhi: New Age International Pvt Ltd Publishers.
[5] Campbell J. (2003). *Castings*. 2nd Edition. Oxford: Butterworth Heinemann.
[6] Mold & Core Test Handbook. (2001). 3rd Edition. Des Plaines, IL: American Foundry Society.
[7] Ettemeyer F., Lechner P., Hofmann T., Andrä H., Schneider M., Grund D., Volk W. & Günther D. (2020). Digital sand core physics: Predicting physical properties of sand cores by simulations on digital microstructures. *International Journal of Solids and Structures*, 188–189, 155–168.
[8] Pittman E.D. (1992). Relationship of porosity and permeability to various parameters derived from mercury injection-capillary pressure curves for sandstone. *AAPG Bulletin*, 76(2), 191–198. Doi: https://doi.org/10.1306/BDFF87A4-1718-11D7-8645000102C1865D.
[9] Dańko R., Dańko J., Burbelko A. & Skrzyński M. (2014). Core Blowing Process – Assessment of Core Sands Properties and Preliminary Model Testing. *Archives of Foundry Engineering*, 14(1), 25–28.
[10] Dańko R. (2017). Influence of the Matrix Grain Size on the Apparent Density and Bending Strength of Sand Cores. *Archives of Foundry Engineering*, 17(1), 27–30.
[11] Kashif M., Cao Y., Yuan G., Asif M., Javed K., Mendez J.N., Khan D. & Miruo L. (2019). Pore size distribution, their geometry and connectivity in deeply buried Paleogene Es1 sandstone reservoir, Nanpu Sag, East China. *Petroleum Science*, 16, 981–1000. Doi: https://doi.org/10.1007/s12182-019-00375-3.
[12] Sundaram D., Svidró J.T., Svidró J. & Diószegi A. (2021). On the Relation between the Gas-Permeability and the Pore Characteristics of Furan Sand. *Materials*, 14(14), 3803. Doi: http://dx.doi.org/10.3390/ma14143803.
[13] Sundaram D., Svidró J.T., Diószegi A. & Svidró J. (2021). Measurement of Darcian Permeability of foundry sand mixtures. *International Journal of Cast Metals Research* 34, 97–103. Doi: https://doi.org/10.1080/13640461.2021.1917890.
[14] Winardi L., Littleton H. & Bates C.E. (2005). New Technique for Measuring Permeability of Cores Made from Various Sands, Binders, Additives and Coatings. *AFS Transactions*, 113, 393–406.
[15] Adams T.C. (1925). Testing Molding Sand to Determine Their Permeability. *AFS Transactions*, 32, 114–167.
[16] Sutherland W. (1893). The viscosity of gases and molecular force. *The London, Edinburgh, and Dublin Philosophical Magazine and Journal of Science*, 36(223), 507–531.
[17] Darcy H.P.G. (1856). *Les Fontaines Publiques de la Ville de Dijon*. Paris: Victor Dalmont.
[18] Rouquerol J., Avnir D., Fairbridge C.W., Everett D.H., Haynes J.M., Pernicone N. & Unger K.K. (1994). Recommendations for the characterization of porous solids (Technical Report). *Pure and Applied Chemistry*, 66(8), 1739–1758.